Numerical Simulation of Inverted Pavement Systems

D. D. Cortes, M.ASCE[1]; H. Shin[2]; and J. C. Santamarina, M.ASCE[3]

Abstract: Conventional pavements rely on stiff upper layers to spread traffic loads onto less rigid lower layers. In contrast, an inverted pavement system consists of an unbound aggregate base compacted on top of a stiff cement-treated base and covered by a relatively thin asphalt concrete layer. The unbound aggregate interlayer in an inverted pavement experiences high cyclic stresses that incite its inherently nonlinear granular media behavior. A physically sound, nonlinear elastoplastic material model is selected to capture the unbound granular base in a finite-element simulator developed to analyze the performance of inverted pavement structures. The simulation results show that an inverted pavement can deliver superior rutting resistance, as compared with a conventional flexible pavement structure with similar fatigue life. **DOI:** **10.1061/(ASCE)TE.1943-5436.0000472.** *© 2012 American Society of Civil Engineers.*

CE Database subject headings: Pavements; Constitutive models; Granular media; Finite element method; Simulation.

Author keywords: Pavement modeling; Constitutive model; Inverted pavement; Particulate media; Finite element; Resilient modulus.

Introduction

Pavement analysis and design combines mechanistic theories and empirical relationships. Layered linear and nonlinear elasticity concepts guided the development of the AASHTO 1972 interim design guide and its subsequent 1993 revision. More recently, underlying concepts are explicitly recognized in the latest mechanistic-empirical pavement design guide developed under the National Cooperative Highway Research Program (NCHRP) Project 1-37A. In this guide, pavement structures are analyzed in two steps. First, the structural response is determined using mechanistic and constitutive material models developed from as-built layer properties; the key results from this analysis are horizontal tensile strains at the bottom/top of the bound aggregate layers and compressive vertical stresses within the unbound layers. Then, these values are used as input parameters to distress prediction models based on accumulated empirical field data, from which the expected pavement life is determined (NCHRP 2004; Kim 2008).

Inverted pavement systems consist of an unbound aggregate base compacted on top of a stiff cement-treated base, covered by a relatively thin asphalt concrete layer. Large cyclic stresses develop within the unbound aggregate layer under service loading, which translate into large transient variations in stiffness during loading-unloading. Linear elastic analyses cannot accommodate the stiffness-stress dependency of unbound aggregate layers and may yield erroneous stress and strain predictions in inverted pavement structures.

The analysis of pavement structures using the finite element method allows for the implementation of constitutive models that can properly capture the nonlinear behavior of unbound aggregate layers. The use of finite elements in the analysis of pavement structures started in the 1960s and led to case-specific codes (Shifley and Monismith 1968; Raad and Figueroa 1980; Brown and Pappin 1981; Barksdale et al. 1989; Harichandran et al. 1990; Brunton and De Almeida 1992; Tutumluer 1995; Park and Lytton 2004). A summary of material models used in previous finite element analyses of flexible pavement structures is presented in Table 1. The general-purpose finite element program ABAQUS has been used to study pavement conditions such as multiple wheel loads, unbound aggregate nonlinear behavior, and anisotropy (Chen et al. 1995; Cho et al. 1996; Hjelmstad and Taciroglu 2000; Sukumaran et al. 2004; Kim et al. 2009). However, material models built in ABAQUS are not suitable to capture the resilient behavior exhibited by unbound aggregate layers.

The objective of this manuscript is to document the development of an ABAQUS-based simulator to analyze the response of inverted pavement systems, including the numerical implementation of a robust constitutive model for the unbound aggregate layer. The simulator is used to guide the selection of the domain size, to reveal the implications of simplifying assumptions, and to identify key differences in the mechanical performance between inverted and conventional flexible pavements.

Pavement Materials: Behavior and Modeling

Asphalt Concrete

The stress-strain behavior of asphalt concrete is determined by the loading frequency, duration and amplitude, temperature, stress state, aging, and moisture (Abbas et al. 2004). Asphalt concrete deforms slowly and permanently at low strain rates and high temperatures and becomes stiffer and brittle at high strain rates and low temperatures (Kim 2008). The tensile strength and strain at failure depend on both temperature and the fraction of air filled void space. Asphalt concrete strength values reported vary between 3.6 and 5.4 MPa at −10°C and 0.9 to 1.6 MPa at 21°C; the strain at failure is on the order of 1×10^{-4} to 3×10^{-3} (Underwood et al. 2005; Kim 2008; Richardson and Lusher 2008). Aggregate shape and compaction during construction result in inherent and stress-induced anisotropy; thus, asphalt concrete exhibits cross-anisotropic

[1]Dept. of Civil Engineering, New Mexico State Univ., Las Cruces, NM (corresponding author). E-mail: dcortes@nmsu.edu

[2]Dept. of Civil and Environmental Engineering, Univ. of Ulsan, Ulsan, South Korea.

[3]Dept. of Civil and Environmental Engineering, Georgia Institute of Technology, Atlanta, GA.

Note. This manuscript was submitted on November 7, 2011; approved on June 13, 2012; published online on November 15, 2012. Discussion period open until May 1, 2013; separate discussions must be submitted for individual papers. This paper is part of the ***Journal of Transportation Engineering***, Vol. 138, No. 12, December 1, 2012. © ASCE, ISSN 0733-947X/2012/12-1507-1519/$25.00.

J. Transp. Eng. 2012.138:1507-1519.

Table 1. Material Models Used in Previous Finite Element Analysis of Flexible Pavement Structures

AC	UAB	Subgrade	CTB	Details	Reference
$t_{AC} = 0.05$ to 0.2 m *Linear elastic*: $E = 4$, 7, and 12 GPa; $\nu = 0.3$	$t_{UAB} = 0.2$ to 0.7 m *Nonlinear elastic cross-anisotropic*: $s_1 = 1/3$; $s_2 = 1$; $\alpha = (8634, 19454\ \text{kPa})$; $\beta = (0.69, 0.5)$; $\gamma = 0$; $\nu = 0.3$	*Linear elastic*: $E = 20$ to 70 MPa $\nu = 0.3$	N/A	Conventional flexible pavements (SENOL) $Q = 500$ kPa, $r = 0.16$ m	Brown and Pappin (1985)
$t_{AC} = 0.09$ m *Linear elastic*: $E = 1720$ MPa; $\nu = 0.35$	$t_{UAB} = 0.2$ m *Nonlinear elastic cross-anisotropic*: $s_1 = 1/3$; $s_2 = 1$; $\alpha = 5367$ psi; $\beta = 0.61$; $\gamma = -0.07$; $E_{Rp} = 0.8\ E_{Rz}$; $\nu_{zp} = 0.43$; $\nu_{pp} = 0.15$	$t_{SG} = 1.27$ m, 1.12 m *Nonlinear elastic*: Bilinear model	$t_{CTB} = 0.15$ m *Linear elastic*: $E = 10340$ MPa $\nu = 0.2$	Axisymmetric Inverted and conventional flexible pavements (GT-PAVE) $Q = 689$ kPa, $r = 0.116$ m	Tutumluer (1995); Tutumluer and Barksdale (1995)
$t_{AC} = 0.05$, to 0.15 m *Nonlinear elastic*: $s_1 = 1/3P_a$; $s_2 = P_a$; $\alpha = 28000$ Pa; $\beta = 0.1$; $\gamma = 0.001$; $\nu = 0.35$	$t_{UAB} = 0.15$ to 0.45 m *Nonlinear elastic cross anisotropic*: $s_1 = 1/3P_a$; $s_2 = P_a$; $\alpha = 3500P_a$; $\beta = (0, 0.455)$; $\gamma = (0, 0.295)$; $\nu_{zp} = 0.2$; $G^* = 0.38E_{Rz}$; $E_{Rp} = (0.5, 1)E_{Rz}$; $\nu_{pp} = 0.3$	$t_{SG} = 2.12$ to 2.52 m Nonlinear elastic $s_1 = 1/3P_a$; $s_2 = P_a$; $\alpha = (207, 1035, 2070)\ P_a$; $\beta = 0.001$; $\gamma = 0.3$; $\nu = 0.35$	NA	Axisymmetric Conventional flexible pavements $Q = 690$ kPa, $r = 0.136$ m, $R = 10r$	Adu-Osei et al. (2001)
$t_{AC} = 0.1$ m *Linear elastic*: $E = 4995.3$ MPa; $\nu = 0.35$ *Nonlinear elastic*: $s_1 = 1/3P_a$; $s_2 = P_a$; $\alpha = 50000$ Pa; $\beta = 0.1$; $\gamma = 0$	$t_{UAB} = 0.2$ m *Linear elastic*: $E = 69.9$ MPa; $\nu = 0.35$ *Nonlinear elastic*: $s_1 = 1/3P_a$; $s_2 = P_a$; $\alpha = 700P_a$; $\beta = 0.6$; $\gamma = -0.3$	$t_{SG} = 1.7$m *Linear elastic*: $E = 40$ MPa; $\nu = 0.4$ *Nonlinear elastic*: $s_1 = 1/3P_a$; $s_2 = P_a$; $\alpha = 400P_a$; $\beta = 0$; $\gamma = -0.3$	N/A	Axisymmetric Conventional flexible pavement sections $Q = 689$ kPa, $r = 0.136$ m, $R = 10r$	Park and Lytton (2004)
$t_{AC} = 0.1$ m *Linear elastic*: $E = 2760$ MPa; $\nu = 0.35$	$t_{UAB} = 0.3$ m *Nonlinear elastic cross-anisotropic*: @170 kPa $E_{Rz} = 25968$, 23088 psi; $E_{Rp} = 5476, 8657$ psi; $G^* = 3815$, 4351 psi;	Linear elastic $E = 20.7$ MPa; $\nu = 0.45$	NA	Conventional flexible pavements (TTI-PAVE) $Q = 1600$ kPa, $r = 0.089$ m	Kim et al. (2005)
$t_{AC} = 0.08$ to 0.127 m *Linear elastic*: $E = 2759$, 8286 MPa; $\nu = 0.35$	$t_{UAB} = 0.2$ to 0.3 m *Nonlinear elastic isotropic*: $s_1 = 1/3P_o$; $s_2 = P_o$; $\nu = (0.38, 0.4)$ $\alpha = (3.5, 4.1, 6.3, 10.3)$ MPa; $\beta = (0.4, 0.635, 0.64)$; $\gamma = (0, 0.01, 0.065)$;	$t_{SG} = 20.8$ to 21 m *Nonlinear elastic*: Bilinear model $\nu = (0.4, 0.45)$	NA	3D-symmetric and axisymmetric Conventional flexible pavements (ABAQUS) $Q = 551$ kPa, $r = 0.152$ m, $R = 20r$	Kim et al. (2009)

Note: $E_R = \alpha\left(\frac{p}{s_1}\right)^{\beta}\left(\frac{q}{s_2}\right)^{\gamma}$, the generic model parameters in the table are valid only for $\sigma_2 = \sigma_3$.

material properties (Underwood et al. 2005). The response of asphalt concrete to service load can be represented by a viscoelastoplastic model (Uzan 2005; Kim 2008).

Cement-Treated Base

The long-term behavior of lightly cemented aggregate bases exhibits three distinctive stages: (1) precracked phase, (2) the onset of fatigue cracking, and (3) advanced crushing. During the precracked phase, the layer behaves as a slab with horizontal plane dimensions larger than the layer thickness; the elastic modulus during this stage corresponds to that measured immediately after construction. At the onset of fatigue cracking, the initial elastic modulus reduces rapidly as the layer breaks down into large blocks with dimensions in the horizontal plane on the order of magnitude of the layer thickness. Finally, in the advanced crushing state, the layer reduces to a granular equivalent with blocks smaller than the layer thickness. At this stage, the originally cemented aggregate now behaves nonlinearly and with stress-dependent stiffness (Theyse et al. 1996; Balbo 1997). This evolution in mechanical behavior of the cement-treated base results in rearrangement of stresses and strains within the entire pavement structure. Therefore, while deterioration of the cemented aggregate itself is not considered a critical mode of distress, it has serious implications on the distress evolution of more critical layers, especially the asphalt concrete layer.

Unbound Aggregate Base and Subgrade Layers

Unbound aggregates exhibit inherently nonlinear behavior. Within a characteristic range of stresses, plastic deformations decrease with the number of load repetitions until only elastic strains are present in the material response, i.e., plastic shakedown. The resilient modulus is defined as the ratio of the repeated load amplitude to the recoverable elastic strain. Experimental studies have established that the resilient response of the granular base is controlled by stress level, density, gradation, particle size, maximum grain size, moisture content, stress history, load duration, and load frequency (Lekarp et al. 2000).

In the plastic shakedown regime, the permanent strain rate per load cycle after the compaction period decreases until the response becomes entirely resilient (Arnold et al. 2002; Werkmeister et al. 2004; García-Rojo and Herrmann 2005; Habiballah and Chazallon 2005; Tao et al. 2010). The resilient modulus increases with the effective confining stress and decreases slightly as the amplitude of the repeated deviator stress increases (Morgan 1966; Hicks and Monismith 1971; Smith and Nair 1973). Dense granular assemblies have high coordination number and resilient modulus (Trollope et al. 1962; Hicks 1970; Robinson 1974; Rada and Witczak 1981; Kolisoja 1997). Density effects are more evident at low values of the mean normal stress (Barksdale and Itani 1989). The stiffness of unbound aggregate layers is also affected by capillary forces (Dawson et al. 1996).

The unbound aggregate base stiffness increases with the fines fraction until the granular skeleton becomes fines-dominated; thereafter, the resilient modulus reduces considerably as the mechanical performance is controlled by the fine aggregate properties (Jorenby and Hicks 1986). Crushed aggregates are characterized by rough angular particles that tend to interlock, forming stronger and stiffer granular assemblies when properly compacted (Allen and Thompson 1974; Thom and Brown 1988; Barksdale et al. 1989; Kim et al. 2005). Aggregate shape also controls the inherent anisotropy of the unbound aggregate base (Pennington et al. 1997).

Numerical Simulator

User-Defined Material Subroutine

A cross-anisotropic nonlinear elastoplastic material model is implemented in Fortran to be inserted as a subroutine in the commercial finite element software ABAQUS. Note that ABAQUS 6.8 uses Fortran 77 code for user subroutines and custom postprocessing applications. Two types of elements are used in the simulations: CPE8R (two-dimensional plane strain) and CAX8R (axisymmetric). Both elements have eight nodes for displacements, and a two-by-two integration point scheme. The notation used in this manuscript follows. Underlined lowercase letters denote second-order tensors, e.g., $\underline{a} = a_{ij}$ (the second-order tensor $\underline{1} = \delta_{ij}$ is the Kronecker delta). Underlined uppercase letters denote fourth-order tensors, e.g., $\underline{A} = A_{ijkl}$; here the $I = (\delta_{ik}\delta_{jl} + \delta_{il}\delta_{jk})/2$ is the unit fourth-order tensor. The symbol ":" denotes the inner product of two tensors; thus, $\underline{a}{:}\underline{b} = a_{ij}b_{ij}$, $\underline{1}{:}\underline{1} = \delta_{ij}$, $\delta_{ij} = 3$, and $\underline{A}{:}\underline{a} = A_{ijkl}a_{kl}$. Finally, the symbol denotes the juxtaposition of two tensors, e.g., $\underline{a} \otimes \underline{b} = a_{ij}b_{kl}$.

The constitutive equations in linear elasticity are represented by the generalized Hooke's law, which can be expressed as $\underline{\sigma} = \underline{D}^e{:}\underline{\varepsilon}$, where $\underline{\sigma} = \sigma_{ij}$ is the stress tensor, $\underline{\varepsilon} = \varepsilon_{ij}$ the strain tensor, and $\underline{D}^e = D^e{}_{ijkl}$ is the fourth-order material stiffness tensor. In cross-anisotropic materials the elastic properties in any direction within the plane perpendicular to a certain axis of symmetry are all the same. Consequently, the stiffness matrix reduces to

$$\underline{D}^e = \begin{bmatrix} \frac{E_{Rp}(E_{Rz}-\nu_{zp}^2 E_{Rp})}{A(1+\nu_{pp})} & \frac{E_{Rp}(\nu_{pp}E_{Rz}+\nu_{zp}^2 E_{Rp})}{A(1+\nu_{pp})} & \frac{\nu_{zp}E_{Rp}E_{Rz}}{A} & 0 & 0 & 0 \\ \frac{E_{Rp}(\nu_{pp}E_{Rz}+\nu_{zp}^2 E_{Rp})}{A(1+\nu_{pp})} & \frac{E_{Rp}(E_{Rz}-\nu_{zp}^2 E_{Rp})}{A(1+\nu_{pp})} & \frac{\nu_{zp}E_{Rp}E_{Rz}}{A} & 0 & 0 & 0 \\ \frac{\nu_{zp}E_{Rp}E_{Rz}}{A} & \frac{\nu_{zp}E_{Rp}E_{Rz}}{A} & \frac{(1-\nu_{pp})E_{Rz}^2}{A} & 0 & 0 & 0 \\ 0 & 0 & 0 & \frac{E_{Rp}}{2(1+\nu_{pp})} & 0 & 0 \\ 0 & 0 & 0 & 0 & G^* & 0 \\ 0 & 0 & 0 & 0 & 0 & G^* \end{bmatrix} \quad (1)$$

where $A = E_{Rz}(1-\nu_{pp}) - 2\nu_{zp}^2 E_{Rp}$; E_{Rp} = Young's modulus in the isotropic plane p; E_{Rz} = Young's modulus in the z-direction normal to the isotropic plane; G^* = shear modulus in the $z-p$ plane; ν_{zp} = Poisson's ratio for stress applied in the z-direction inducing strains in the p-direction; and ν_{pp} = Poisson's ratio for stress applied in a p-direction inducing strains in the p-plane.

Constitutive Model

Robust model predictions start with the physically guided selection of the material model to satisfy experimental observations. While a large number of model parameters favors data fitting, we follow Ockham's rule of parsimony, i.e., the simplest model that properly justifies the data (Santamarina and Fratta 2005); hence, we seek a physically sound, simple model that can adequately justify the data. In particular, the selected model must capture (1) the Hertzian-type stress-dependent stiffness of unbound granular bases and (2) the skeletal softening caused by deviatoric loads that approach failure. The model initially proposed by Huurman (1996) and later modified by Van Niekerk et al. (2002) satisfies these fundamental criteria:

$$E_R = k_1 \left(\frac{p}{p_0}\right)^{k_2} \left[1 - k_3 \left(\frac{q}{q_f}\right)^{k_4}\right] \tag{2}$$

where

$$p = \frac{1}{3}\underset{\sim}{\sigma}:\underset{\sim}{1}, \qquad q = \sqrt{\frac{3}{2}\underset{\sim}{\sigma}':\underset{\sim}{\sigma}'\underset{\sim}{1}} \text{ and } \underset{\sim}{\sigma}' = \underset{\sim}{\sigma} - p\underset{\sim}{1}$$

and p = mean stress; q = deviatoric stress; q_f = deviatoric stress at failure, and p_o = normalizing stress. This nonlinear elastic model consists of two stress terms and four fitting parameters: k_1 = resilient modulus at $p = p_o$ and $q = 0$; $k_2 > 0$ captures the sensitivity of the resilient modulus to the mean stress; and $k_3 > 0$ and $k_4 > 0$ combine to capture skeletal softening induced by the deviator stress q in reference to the proximity to the failure load q_f. Guidance for the determination of physically meaningful k_2 values can be found in the elastic wave velocity literature (Kopperman et al. 1982; Hardin and Blandford 1989; Santamarina et al. 2001). The values of k_2 can range from $k_2 = 0$ for cemented soils to $k_2 = 1.5$ in soils whose response is strongly influenced by electrical interactions. In the case of unbound aggregates used for pavement bases and subbases, expected values can be found in a range from $k_2 = 0$ for cement-treated bases to 0.5 for rough/angular aggregates.

The deviatoric stress softening effect is controlled by k_3 and k_4. At $q = q_f$, the material reaches failure, and the stress softening term reduces to $1 - k_3$; thus, physically meaningful values of k_3 are in a range of $k_3 = 0$ (no softening) to $k_3 = 1$ (flow at failure). The k_4 parameter captures the softening sensitivity of the material for a given deviatoric stress amplitude. Stiffness diminishes linearly with deviatoric loading if $k_4 = 1$. Typically, the effect of deviatoric loading is low when $q << q_f$ and increases as the material approaches failure; therefore $k_4 > 1$. The selected model can also be extended to capture cross-anisotropic material behavior as follows:

$$E_{Rp} = k_1 \left(\frac{p}{p_0}\right)^{k_2} \left[1 - k_3 \left(\frac{q}{q_f}\right)^{k_4}\right] \tag{3}$$

$$E_{Rz} = k_5 \left(\frac{p}{p_0}\right)^{k_6} \left[1 - k_7 \left(\frac{q}{q_f}\right)^{k_8}\right] \tag{4}$$

$$G^* = k_9 \left(\frac{p}{p_0}\right)^{k_{10}} \left[1 - k_{11} \left(\frac{q}{q_f}\right)^{k_{12}}\right] \tag{5}$$

The limiting failure strength q_f is recognized in the model so that modeled loads result in a state of stresses compatible with failure conditions. Here, the Drucker-Prager failure criterion is applied to determine the boundary between elastic and perfectly plastic deformations, which follow an associated flow rule. The failure surface f is a function of the material strength parameters, i.e., friction angle ϕ and apparent cohesion c, with no hardening. The onset of plastic deformation is defined by $f = 0$. The material remains in the elastic regime as long as $f < 0$ and deforms plastically for $f = 0$. The state of stresses at failure is given by

$$q_f = \frac{6\cos\phi}{3 - \sin\phi} c + \frac{6\sin\phi}{3 - \sin\phi} p \tag{6}$$

Plastic behavior is incorporated in the user-defined material subroutine through a continuum tangent modulus formulation. The elastoplastic stress-strain relationship is given by

$$\dot{\underset{\sim}{\sigma}} = \underset{\sim}{D}^{\mathrm{ep}}:\dot{\underset{\sim}{\varepsilon}} = (\underset{\sim}{D}^e - a\underset{\sim}{b} \otimes \underset{\sim}{d}):\dot{\underset{\sim}{\varepsilon}} \tag{7}$$

where

$$a = \frac{1}{\left(\underset{\sim}{n} - \frac{\sqrt{2}}{3\sqrt{3}}\xi\underset{\sim}{1}\right):\underset{\sim}{D}^e:\left(\underset{\sim}{n} - \frac{\sqrt{2}}{3\sqrt{3}}\xi^*\underset{\sim}{1}\right)}$$

$$\underset{\sim}{b} = \underset{\sim}{D}^e:\left(\underset{\sim}{n} - \frac{\sqrt{2}}{3\sqrt{3}}\xi^*\underset{\sim}{1}\right)$$

$$\underset{\sim}{d} = \underset{\sim}{D}^e:\left(\underset{\sim}{n} - \frac{\sqrt{2}}{3\sqrt{3}}\xi\underset{\sim}{1}\right)$$

$$\xi = \frac{6\sin\phi}{3 - \sin\phi} \qquad \xi^* = \frac{6\sin\delta}{3 - \sin\delta} \qquad \underset{\sim}{n} = \frac{\underset{\sim}{\sigma}'}{\|\underset{\sim}{\sigma}'\|}$$

The stress increment $\dot{\underset{\sim}{\sigma}}$ is defined in terms of the strain increment $\dot{\underset{\sim}{\varepsilon}}$, the elastic stiffness tensor $\underset{\sim}{D}^e$, the friction angle ϕ, and the dilation angle δ.

Code Verification

The verification of the user-defined material subroutine is done by comparison with existing models including Boussinesq close-form solution, standard ABAQUS material models, and published results obtained for multilayered linear elastic pavement analysis software packages. Note that the implemented cross-anisotropic nonlinear material model reduces to linear elasticity by using appropriate input parameters (Table 2). The geometric parameters and loads summarized in Table 2 refer to the dimensions and distributed loads shown in Fig. 1(a). Parameters for nonlinear analyses are extracted by fitting constant confinement cyclic triaxial test data using the proposed constitutive model and the material subroutine.

Isotropic Linear Elasticity

A 103 kPa uniformly distributed load is applied over a circular area of $r = 0.13$ m diameter on an isotropic linear elastic material with $E = 200$ MPa and a $\nu = 0.3$. Boussinesq and numerical predictions superimpose as shown in Fig. 2(a).

Multilayered Isotropic Linear Elasticity

A conventional flexible pavement structure [Fig. 1(a)] is modeled using the isotropic linear elastic properties reported in simulations by Tutumluer (1995). Young's modulus and Poisson's ratio values for the different layers are presented in Table 2. Predicted vertical stresses along the centerline caused by a 103 kPa uniformly

J. Transp. Eng. 2012.138:1507-1519.

Table 2. Numerical Simulator Verification and Validation Parameters

Figure	Load/geometry	Property	Parameter
2(a)	$Q = 103$ kPa $R = 1.3$ m $r = 0.127$ m $t = 2.54$ m	$E = 200$ MPa $\upsilon = 0.3$	$k_1 = k_5 = 200$ MPa; $k_9 = 76.9$ MPa $k_2 = k_3 = k_4 = k_6 = k_7 = k_8 = k_{10} = k_{11} = k_{12} = 0$ $\nu_{pp} = \nu_{zp} = 0.3$; $p_0 = 1$ kPa
2(b)	$Q = 103$ kPa $R = 1.3$ m $r = 0.127$ m $t_{AC} = 0.1$ m $t_{UAB} = 0.28$ m $t_{SG} = 2.54$ m	AC: $E = 2000$ MPa $\upsilon = 0.35$ UAB: $E = 310$ MPa $\upsilon = 0.45$ SG: $E = 50$ MPa $\upsilon = 0.4$	AC: $k_1 = k_5 = 2000$ MPa; $k_9 = 741$ MPa $k_2 = k_3 = k_4 = k_6 = k_7 = k_8 = k_{10} = k_{11} = k_{12} = 0$ $\nu_{pp} = \nu_{zp} = 0.35$; $p_0 = 1$ kPa UAB: $k_1 = k_5 = 310$ MPa; $k_9 = 107$ MPa $k_2 = k_3 = k_4 = k_6 = k_7 = k_8 = k_{10} = k_{11} = k_{12} = 0$ $\nu_{pp} = \nu_{zp} = 0.45$; $p_0 = 1$ kPa SG: $k_1 = k_5 = 50$ MPa; $k_9 = 17.9$ MPa $k_2 = k_3 = k_4 = k_6 = k_7 = k_8 = k_{10} = k_{11} = k_{12} = 0$ $\nu_{pp} = \nu_{zp} = 0.4$; $p_0 = 1$ kPa
2(c)	$Q = 103$ kPa $R = 1.3$ m $r = 0.127$ m $t_{AC} = 0.1$ m $t_{UAB} = 0.28$ m $t_{SG} = 2.54$ m	AC: $E = 2000$ MPa $\upsilon = 0.35$ UAB: $E_{Rz} = 310$ MPa $E_{Rp} = 46.5$ MPa $G^* = 108$ MPa $\upsilon_{pp} = 0.15$ $\upsilon_{zp} = 0.45$ SG: $E = 50$ MPa $\upsilon = 0.4$	AC: $k_1 = k_5 = 2000$ MPa; $k_9 = 741$ MPa $k_2 = k_3 = k_4 = k_6 = k_7 = k_8 = k_{10} = k_{11} = k_{12} = 0$ $\nu_{pp} = \nu_{zp} = 0.35$; $p_0 = 1$ kPa UAB: $k_1 = 310$ MPa; $k_5 = 46.5$ MPa; $k_9 = 108$ MPa $k_2 = k_3 = k_4 = k_6 = k_7 = k_8 = k_{10} = k_{11} = k_{12} = 0$ $\nu_{pp} = 0.15$; $\nu_{zp} = 0.45$; $p_0 = 1$ kPa SG: $k_1 = k_5 = 50$ MPa; $k_9 = 17.9$ MPa $k_2 = k_3 = k_4 = k_6 = k_7 = k_8 = k_{10} = k_{11} = k_{12} = 0$ $\nu_{pp} = \nu_{zp} = 0.4$; $p_0 = 1$ kPa
3	$R = r = 0.0762$ m $t = 0.304$ m	$E_{Rz} = E_{Rz}(p, q)$	$k_1 = 32.8$ MPa; $k_5 = 32.8$ MPa; $k_9 = 12.3$ MPa $k_2 = k_6 = k_{10} = 0.5$ $k_3 = k_7 = k_{11} = 0.9$ $k_4 = k_8 = k_{12} = 16$ $\nu_{pp} = \nu_{zp} = 0.33$ $p_0 = 1$ kPa; $\varphi = 40°$; $C = 1$ kPa

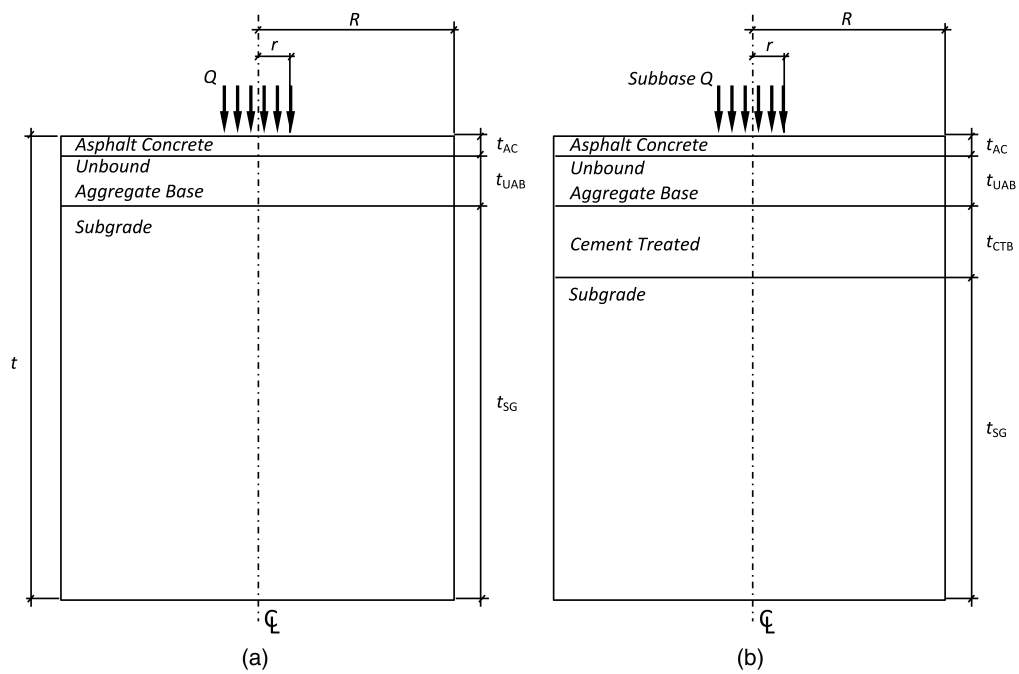

Fig. 1. (a) Conventional flexible pavement; (b) inverted pavement structures

distributed load favorably compare to predictions made by KENLAYER and GT-Pave (Tutumluer 1995) in Fig. 2(b). (Note: minor discrepancies between KENLAYER and GT-Pave are in part due to data digitization from published plots.)

Multilayered Cross-Anisotropic Linear Elasticity

Predictions using the new code for cross-anisotropic linear behavior are compared to published results obtained with GT-Pave (Tutumluer 1995) in Fig. 2(c). The asphalt concrete and the subgrade are modeled as isotropic linear elastic layers using the same properties as in Fig. 2(b). The unbound aggregate layer is modeled as a cross-anisotropic linear elastic layer (parameters in Table 2).

Summary

The three verification studies show that the predictions made using the proposed user-defined material model subroutine agree with closed-form solutions and established multilayered linear elastic isotropic and cross-anisotropic simulators.

J. Transp. Eng. 2012.138:1507-1519.

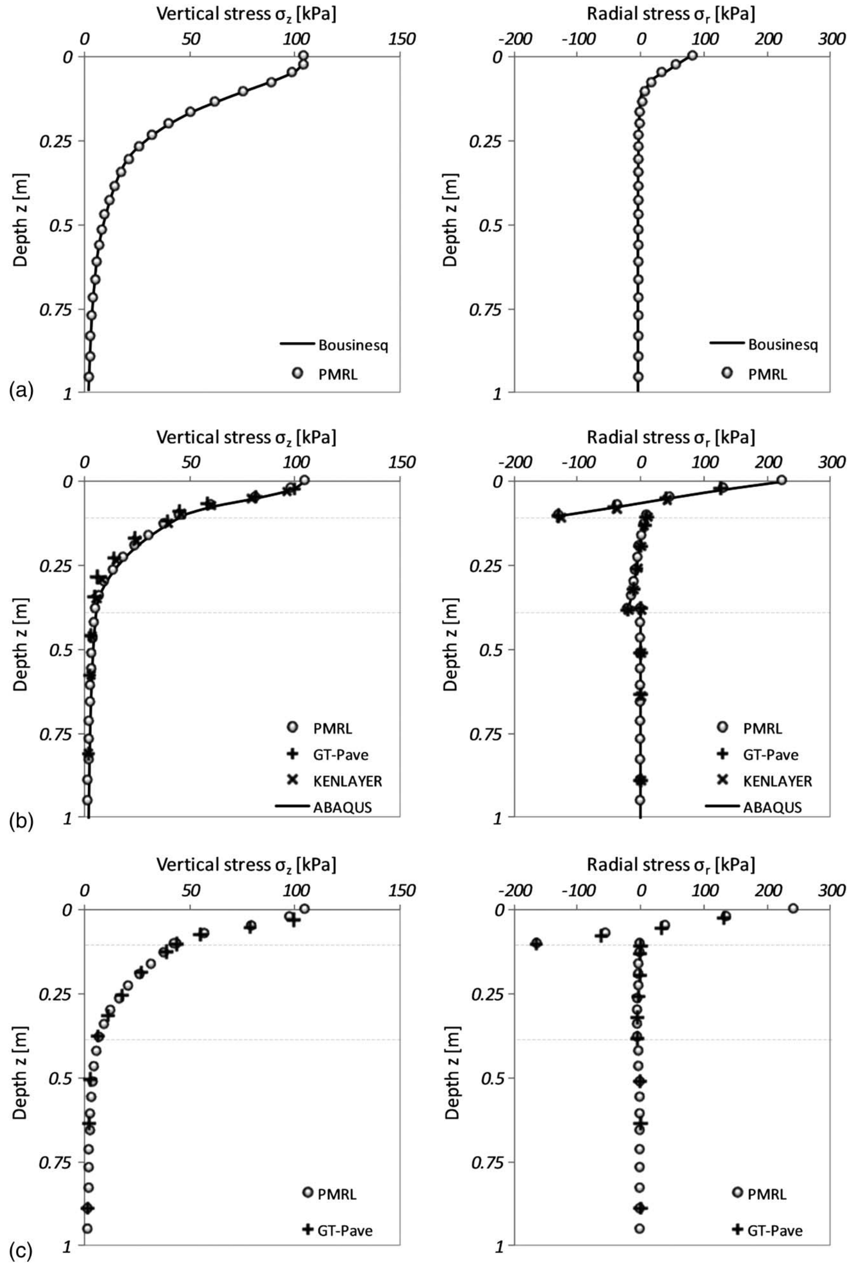

Fig. 2. Particulate media research laboratory (PMRL) model validation studies: (a) isotropic linear elastic half-space subjected to a circular uniform load; (b) layered isotropic linear elastic solutions from available pavement analysis software; (c) layered cross-anisotropic linear elastic base solutions from GT-Pave; results presented for KENLAYER and GT-Pave were digitized from Tutumluer (1995)

Model Calibration

Constant confinement cyclic triaxial test results for a crushed Georgia granite aggregate reported in Tutumluer (1995) are used to assess the ability of the model to reproduce the physical response of unbound aggregate layers. Tests were conducted at five different cell pressures and three deviatoric stress increments for each cell pressure. The procedure followed for the determination of the constitutive model k_i parameters satisfies physical constraints derived from soil mechanics; k_i values are summarized in Table 2. There is very good agreement between numerical model predictions and the experimental data, as shown in Fig. 3.

Domain Size and Boundary Conditions

Previous numerical and experimental studies show that zero displacement boundaries must be far from the loaded area to minimize boundary effects (e.g., Kim 2007; Kim et al. 2009). A numerical investigation was conducted to assess boundary effects on the predicted mechanical response of an inverted pavement structure. Following the recommendations of the guide for mechanistic-empirical design of new and rehabilitated pavement structures (NCHRP 2004), a 550 kPa tire contact pressure spread over a circular area of radius 0.15 m is used. The domain dimensions and material properties of individual layers are summarized in Table 3. The pavement section is modeled using a 3D axisymmetric mesh that replicates the geometry of the inverted pavement structure shown in Fig. 1(b). It is assumed that there is no slip at the interfaces between layers. Results presented in Fig. 4 show the sensitivity of critical design parameters including effects on maximum tensile strains in the asphalt concrete and cement-treated base and maximum vertical compressive stresses in the unbound aggregate base and subgrade to variations in the horizontal domain R/r.

J. Transp. Eng. 2012.138:1507-1519.

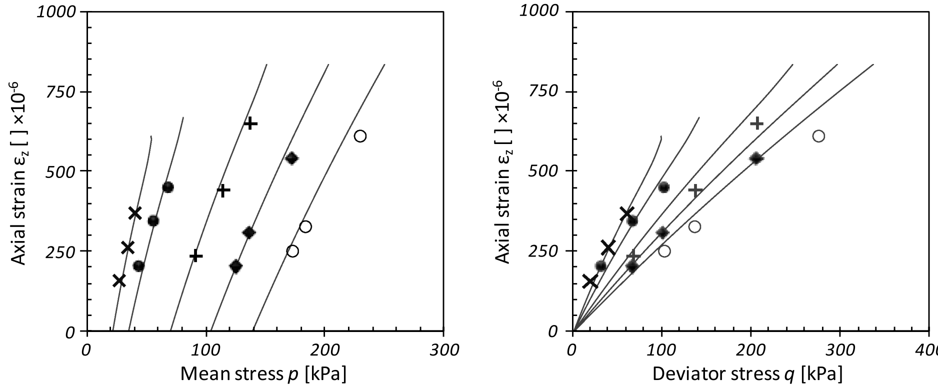

Fig. 3. Nonlinear elastic model validation using repeated load triaxial test results for crushed granite from Georgia (data in Tutumluer 1995)

Table 3. Material Properties and Layer Dimensions

Layer	Material model
Asphalt concrete ($t_{AC} = 0.09$ m)	*Isotropic linear elastic* $E = 1.7$ GPa $\nu = 0.35$
Unbound aggregate base ($t_{\mathrm{UAB}} = 0.15$ m)	*Isotropic nonlinear elastoplastic* $E_{Rz} = 200\ \mathrm{MPa} \cdot \left(\frac{p}{1\ \mathrm{kPa}}\right)^{0.2}\left[1 - 0.9 \cdot \left(\frac{q}{q_f}\right)^{16}\right]$ $E_{Rp} = 200\ \mathrm{MPa} \cdot \left(\frac{p}{1\ \mathrm{kPa}}\right)^{0.2}\left[1 - 0.9 \cdot \left(\frac{q}{q_f}\right)^{16}\right]$ $G^* = 76.9\ \mathrm{MPa} \cdot \left(\frac{p}{1\ \mathrm{kPa}}\right)^{0.2}\left[1 - 0.9 \cdot \left(\frac{q}{q_f}\right)^{16}\right]$ $\nu_{pp} = \nu_{zp} = 0.3$ $\varphi = 40°$; $C = 1$ kPa
Cement-treated base ($t_{\mathrm{CTB}} = 0.25$ m)	*Isotropic linear elastic* $E = 13.7$ GPa $\nu = 0.2$
Subgrade ($t_{\mathrm{SG}} = 2.54$ m)	*Isotropic linear elastic* $E = 100$ MPa $\nu = 0.2$

The influence of the lateral boundary was assessed by imposing a zero-lateral-displacement boundary along the edge of the model for all layers [Figs. 4(a and c)] and only along the unbound aggregate base and subgrade layers [Figs. 4(b and d)]. There are only minor differences in the magnitude of the parameters studied in part due to the prescribed no-slip interfaces. In both cases, boundary effects are minimal when $R/r > 20$. There is a 30% difference in predicted maximum tensile strains in the cement-treated base and a 15% difference in the predicted maximum compressive stress in the subgrade between $R/r = 10$ and 20.

The proximity of the wheel to the road often creates a range of physically meaningful domain sizes between $R/r = 5$ and 10. Results in Fig. 4 show that simulations with a domain size $R/r \geq 20$ can lead to a 140% underestimation of the maximum compressive stress in the subgrade, a 60% overestimation of the maximum tensile strain in the cement-treated base, and a 6% overestimation of the maximum tensile strain in the asphalt concrete layer. Consequently, predictions made using $R/r \geq 20$ would underestimate subgrade rutting, the fatigue resistance of the cement-treated base and the fatigue life of the asphalt concrete layer. The rest of the study is conducted with an intermediate value of $R/r = 10$.

Modeling of Anisotropy

The influence of anisotropic material properties is examined via a parametric numerical study of triaxial and zero-lateral-strain loading simulations. Anisotropic elements are created using three values for the initial vertical to horizontal stiffness [i.e., k_5/k_1 as defined in Eqs. (2) and (3)] 0.5, 1, and 1.5. This is implemented by assigning parameter k_5 values of 100, 200, and 300 MPa while maintaining all other parameters constant (Table 3). Note that k_1 and k_5 represent the vertical and horizontal resilient moduli at the reference stress p_o, respectively. Thus, the ratio k_1/k_5 captures the level of anisotropy at the reference stress. Numerical simulation results are presented in Fig. 5(a) for triaxial loading simulations and Fig. 5(b) for zero-lateral-strain loading simulations. The results of triaxial loading simulations show that when $k_5/k_1 < 1$, i.e., $k_5 = 100$ MPa, the material behaves elastically over a broader range of vertical strains. The opposite occurs when $k_5/k_1 > 1$, i.e., $k_5 = 300$ MPa. The results of zero-lateral-strain loading simulations are presented in terms of the horizontal-to-vertical-stress ratio, also known as k_o. Minor differences are observed in the value of k_o at very low vertical strains ($\varepsilon_z < 5 \times 10^{-5}$). However, as the vertical strain increases, k_o varies distinctively for each k_5/k_1, progressing toward a particular asymptotic value at large strains ($\varepsilon_z > 1 \times 10^{-3}$).

Simulation Studies and Results

Three simulation studies are conducted to explore the mechanical performance of an inverted pavement structure, to study the impact of simplifying assumptions, and to identify an equivalent conventional flexible pavement structure for a preselected inverted pavement.

Mechanical Performance of an Inverted Pavement Structure

This simulation study is conducted to determine the mechanical response, stresses and strains, of the inverted pavement structure depicted in Fig. 1(b) (layer thicknesses in Fig. 6). Following the findings on domain size reported previously, we model the load on the pavement as a 550 kPa tire contact pressure spread over a circular area of radius $r = 0.15$ m with a domain size $R = 10$ $r = 1.50$ m. Material properties and layer thicknesses are summarized in Table 3. The pavement structure is modeled using a 3D axisymmetric edge biased mesh, with zero-lateral-displacement boundaries at the edge of the pavement, zero vertical displacement at the lower boundary, and no-slip between the layers.

The resulting vertical, radial, and shear stress distributions along the centerline and under the wheel edge are presented in Fig. 6. Vertical stresses along the centerline and the wheel edge are compressive throughout the full depth of influence of the load and become negligible within the cement-treated base. Radial stresses along the centerline and wheel line for the asphalt concrete and cement-treated base layers range from compression at the top to

J. Transp. Eng. 2012.138:1507-1519.

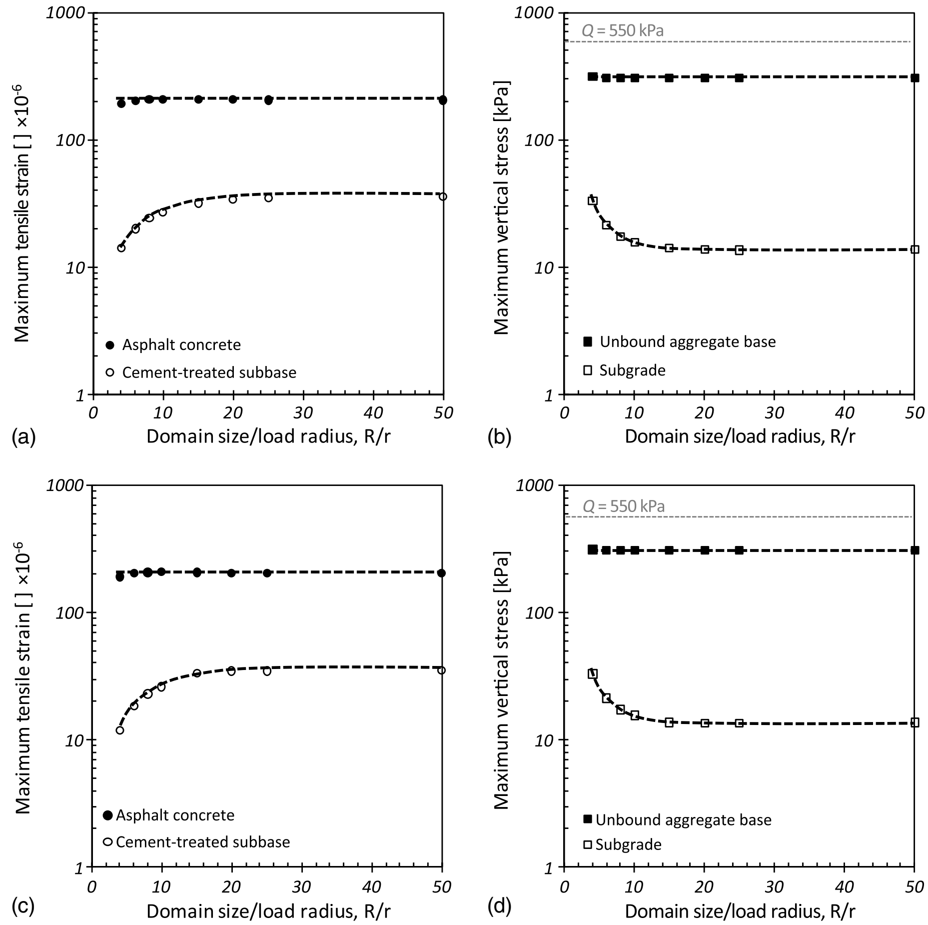

Fig. 4. Effects of model domain size and choice of boundary conditions on critical pavement design parameters for an inverted pavement structure: (a) and (c) maximum tensile strains in asphalt concrete ε_{AC} and cement-treated base ε_{CTB} layers; (b) and (d) maximum vertical stress on unbound aggregate base σ_{UAB} and subgrade σ_{SG} layers; zero lateral displacement boundaries are used along the edge of the model for all layers in (a) and (c) and along the unbound aggregate base and subgrade only in (b) and (d)

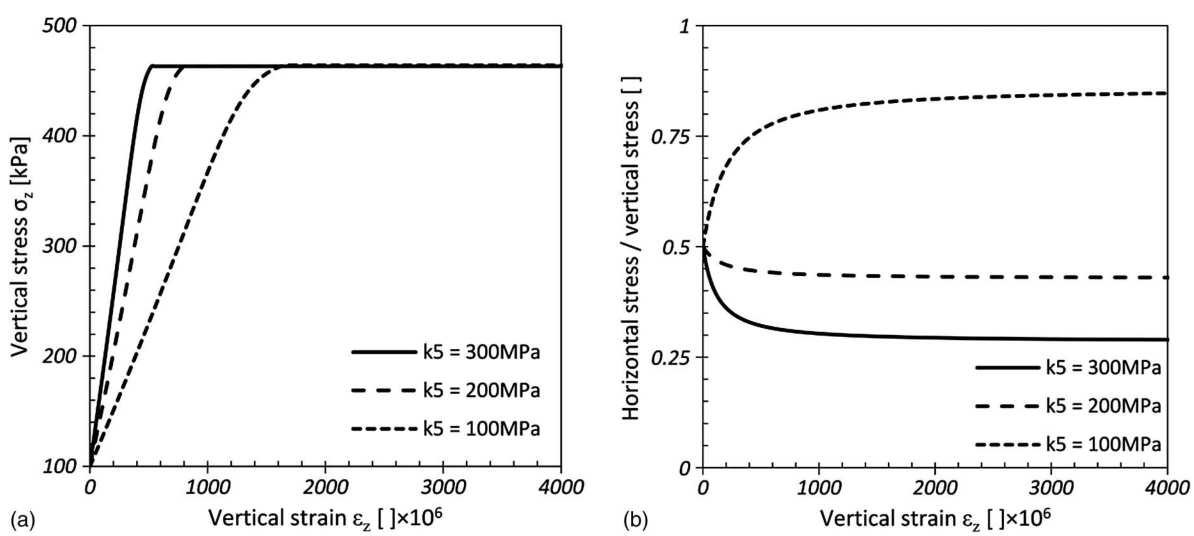

Fig. 5. Effect of anisotropic material behavior on stress-strain response for different types of strain loading: (a) triaxial; (b) zero-lateral-strain

tension at the bottom. Both vertical and radial stresses in the unbound aggregate base remain in compression for the full depth of the layer (in agreement with imposed Mohr-Coulomb behavior). Shear stresses are zero along the centerline and reach maximum values along the wheel edge. The maximum shear stress along the wheel edge occurs within the asphalt concrete layer.

Radial slices of the vertical stress field are shown at multiple depths in Fig. 7(a). The vertical stress caused by the wheel load

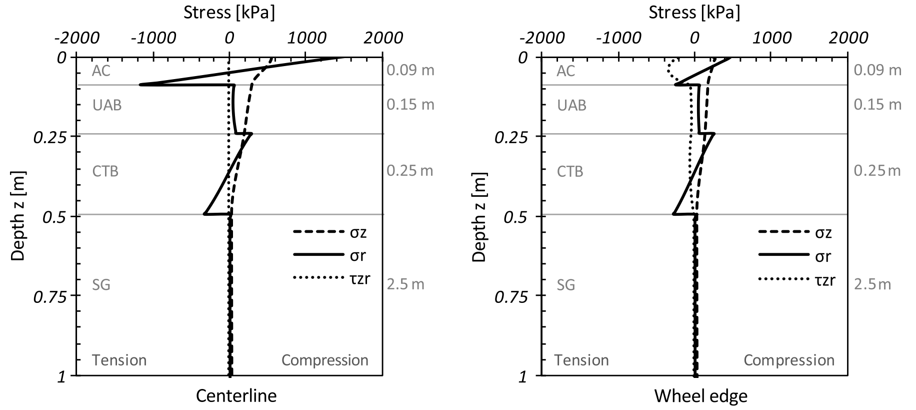

Fig. 6. Vertical σ_z, radial σ_r, and shear τ_{zr} stress profiles as a function of depth in modeled inverted pavement structure along load centerline and wheel edge for a 550 kPa uniformly distributed load over a circular area of radius 0.15 m

diminishes with depth; the peak vertical stress on the subgrade is less than 4% of the vertical stress applied on the surface. Slices of the horizontal and shear stress fields at different depths are presented in Figs. 7(b and c). Radial tensile stresses in the asphalt layer are greatest along the bottom of the layer, reaching a maximum at the load centerline. The unbound aggregate base cannot sustain tensile stresses; therefore, the constitutive model correctly predicts compressive stresses along the bottom of the unbound aggregate base. Tensile stresses at the bottom of the cement-treated base also reach a maximum at the centerline. The shear stresses along the asphalt concrete surface show a peak at the wheel edge, where there is a large discontinuity in vertical stresses. In the unbound aggregate layer, shear stresses increase slightly with depth along the wheel edge. The cement-treated base considerably reduces the wheel-induced shear stresses on the subgrade.

Linear Elastic Unbound Aggregate Layer Modeling Implications

The use of linear elastic models for the analysis of conventional pavement structures, i.e., with decreasing layer stiffness with depth, predicts tensile stresses at the bottom of the asphalt concrete layer, the unbound aggregate base, and the subbase. However, linear elastic analysis of inverted pavement structures does not predict tensile stresses in the unbound aggregate base because the stiffness profile characteristic of inverted pavement structures results in the development of compressive stresses along the full thickness of the unbound aggregate base.

Additional implications of using simple linear elastic models to represent the unbound aggregate base in the analysis of an inverted pavement structure are identified by comparing the results of the nonlinear elastoplastic material model (NLEP) with two linear elastic models: (1) LE1 has a Young's modulus of 230 MPa corresponding to the in-situ measured unloaded unbound aggregate base stiffness, and (2) LE2 has a Young's modulus of 500 MPa corresponding to the model predictions for the state of stresses at mid-depth in the unbound aggregate base, under a 550 kPa wheel load. The results of the three analyses are shown in Fig. 8; differences between linear and nonlinear analyses follow:

1. The maximum tensile strain at the bottom of the asphalt concrete layer is underestimated by 33% when the maximum elastic modulus is used and overestimated by 5% when the minimum elastic modulus is used.
2. The maximum tensile strain at the bottom of the cement-treated base is underestimated by 4% when the maximum

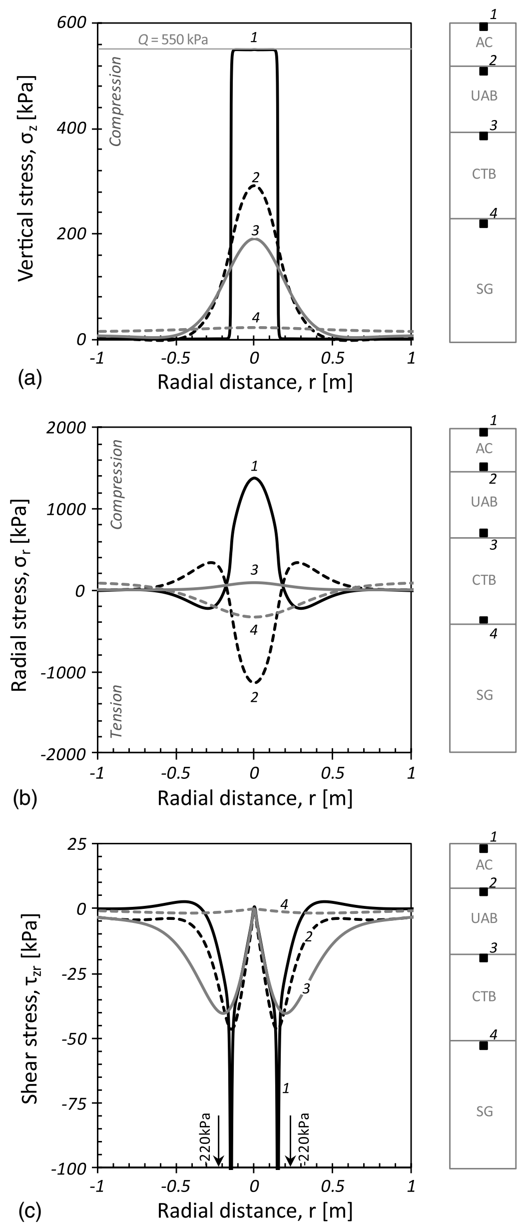

Fig. 7. Radial profiles of (a) vertical, (b) radial, and (c) shear stresses at multiple locations within inverted pavement structure; $Q = 550$ kPa, $r = 0.15$ m, $R = 10r$

J. Transp. Eng. 2012.138:1507-1519.

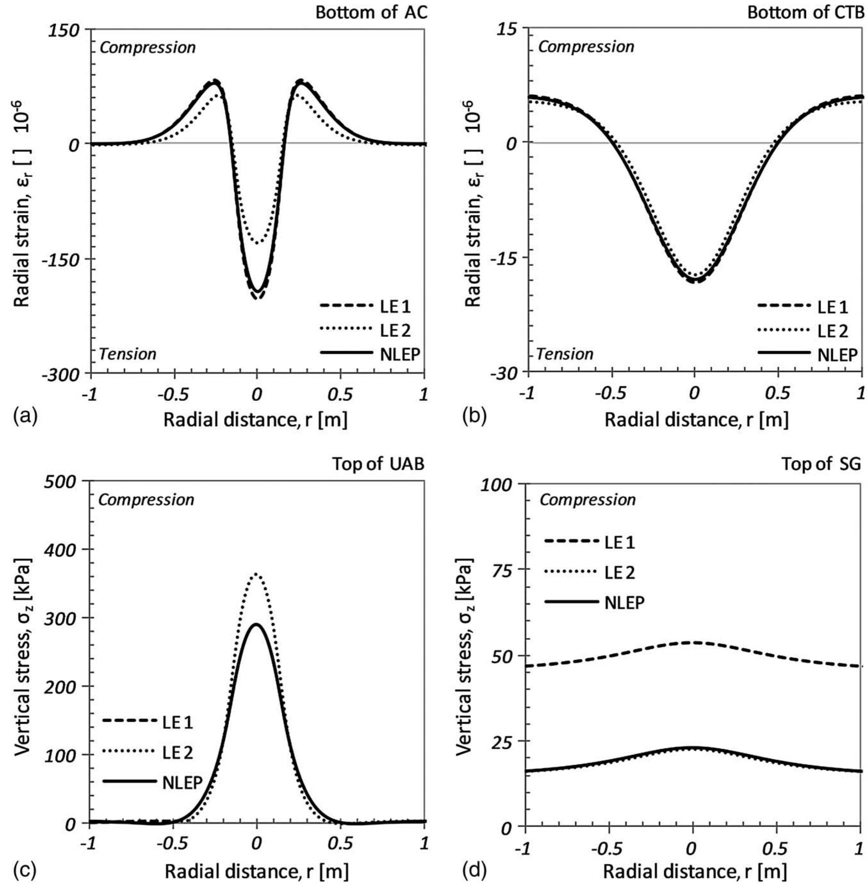

Fig. 8. Comparison between inverted pavement critical design parameter predictions from linear elastic and nonlinear elastoplastic unbound aggregate base models: (a) strains at bottom of asphalt concrete layer; (b) strains at bottom of cement-treated base layer; (c) vertical stresses on top of unbound aggregate base layer; (d) vertical stresses on top of subgrade layer; $Q = 550$ kPa, $r = 0.15$ m, $R = 10r$

elastic modulus is used and overestimated by 2% when the minimum elastic modulus is used.

3. The maximum compressive stress on the unbound aggregate base is overestimated by 25% when the maximum elastic modulus is used.
4. The maximum compressive stress on the subgrade is overestimated by 135% when the minimum elastic modulus is used.

As a corollary, we note that the tensile stresses in the asphalt concrete layer and in the cement-treated base, as well as the compressive stress on the subgrade, increase as the stiffness of the unbound granular base decreases.

Equivalent Conventional Flexible Pavement Study

We use successive forward simulations to identify a conventional flexible pavement of similar mechanical performance to the studied inverted pavement. The simulation assumes that the material properties of individual layers are the same in the conventional and inverted sections (Table 3). The mechanical response is compared in terms of the critical design parameters for fatigue failure analysis (i.e., maximum tensile strain at the bottom of the asphalt concrete) and rutting failure analysis (i.e., maximum vertical stress on the subgrade).

The mechanical response of the studied inverted pavement and three conventional flexible pavement structures are compared in Fig. 9. To facilitate the comparison, we keep the thickness of the unbound aggregate base constant in all of the conventional pavement structures. Simulation results show that a conventional pavement section with asphalt concrete thickness $t_{AC} = 0.17$ m and an unbound aggregate base thickness $t_{UAB} = 0.3$ m sustains similar maximum tensile strain in the asphalt concrete layer as the inverted pavement. However, the inverted pavement is more efficient in redistributing the vertical compressive stresses transferred to the subgrade.

Discussion

Mechanical Performance

The vertical stress profile presented in Fig. 7(a) shows that the compressive vertical stresses along the centerline decrease from the applied wheel load 550 kPa on top of the asphalt concrete, to 190 kPa at the top of the cement-treated base. The maximum tensile radial stress is 1380 kPa at the bottom of the asphalt concrete and 330 kPa at the bottom of the cement-treated base [Fig. 7(b)]. The maximum tensile stress in the asphalt concrete layer (Fig. 6) is between 0.4 and 0.6 of the material tensile strength for the simulated load (e.g., Richardson and Lusher 2008). The predicted maximum tensile strain 1.9×10^{-4} is in the range measured for inverted pavement test sections built with similar materials and geometry ($2.6 \times 10^{-4} \sim 3.4 \times 10^{-4}$; Tutumluer and Barksdale 1995) and resembles the strain level in a conventional flexible pavement with an asphalt concrete layer twice as thick.

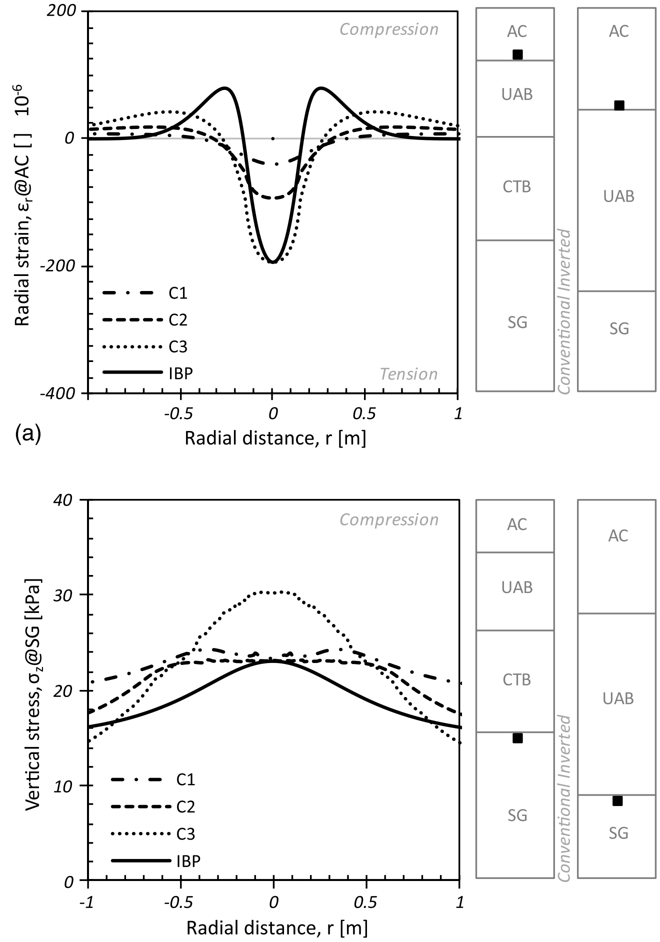

	t_{AC} [m]	t_{UAB} [m]	t_{CTB} [m]
C1	0.38	0.30	0
C2	0.25	0.30	0
C3	0.17	0.30	0
IBP	0.09	0.15	0.25

(b)

Fig. 9. Mechanical response in terms of (a) tensile strains at bottom of asphalt concrete layer and (b) vertical stresses on subgrade for studied inverted pavement structure and three conventional flexible pavement structures; wheel load $Q = 550$ kPa, contact area radius $r = 0.15$ m, domain size $R = 10r$

Linear Elastic Unbound Aggregate Material Models

The stiffness profile characteristic of an inverted pavement structure prevents the generation of tensile stresses in the unbound aggregate base regardless of the material model assigned to the unbound aggregate base (linear or nonlinear elastic). A linear elastic analysis based on the maximum expected modulus yields conservative unbound aggregate base rutting predictions, but nonconservative asphalt concrete and cement-treated base fatigue predictions. A linear elastic analysis based on the minimum expected stiffness leads to better asphalt concrete and cement-treated base fatigue predictions but significantly overestimates subgrade rutting.

Equivalent Section

Limited comparative results of equivalent sections show a superior performance of the inverted pavement in terms of subgrade rutting prevention (lower peak vertical stress on the subgrade) for the same maximum tensile strain in the asphalt concrete layer (i.e., equal fatigue life). However, thin asphalt concrete layers are prone to shear failure and top-down cracking due to the stresses along the wheel edge.

The unbound aggregate material properties will not be the same in inverted and conventional flexible pavement structures. The aggregate base in inverted pavement systems can reach higher density because of the support provided by the stiff cement-treated base during compaction. Therefore, the as-built unbound aggregate base in an inverted pavement structure may exhibit higher stiffness and lower long-term stiffness-degradation than the aggregate base in a conventional flexible pavement.

It follows from this discussion that (1) the material parameters used to model the unbound aggregate base in an inverted pavement and a conventional flexible pavement may vary for the same aggregate, (2) the empirical fatigue and rutting distress prediction models developed for conventional flexible pavements are prone to yield conservative estimates of pavement life for inverted pavement structures (differences in stiffness degradation), and (3) the design of inverted pavement structures requires the analysis of additional failure mechanisms and critical mechanical response parameters.

Conclusions

The unbound aggregate layer in an inverted base pavement experiences large cyclic stresses under service loading; this translates into large transient variations in stiffness during load-unload cycles.

The analysis of pavement structures using the finite element method allows for the implementation of constitutive models that can properly reproduce the observed behavior of unbound aggregate layers. The selected model captures the Hertzian-type stress-dependent stiffness of unbound granular bases and the skeletal softening caused by deviatoric loads that approach failure. It is fitted to data using four physically meaningful and experimentally accessible constitutive parameters.

Simulation results show that the stiffness profile in inverted pavement structures prevents the development of tensile stresses in the unbound aggregate base even if a linear model is used to represent it.

While linear elastic analyses cannot accommodate the stiffness-stress dependency of unbound aggregate layers, limiting conditions can be simulated using an elastic response by adopting the in-situ stiffness before load application and the stiffness under maximum load.

The maximum vertical compressive stress in the subgrade of an inverted pavement is lower than the value predicted for a conventional flexible pavement structure designed to experience the same maximum strain in the asphalt concrete layer. Thus, the inverted pavement will deliver superior rutting resistance.

The presence of a stiff cement-treated base facilitates the compaction of the unbound aggregate base so that the as-built stress-dependent stiffness of the unbound aggregate base will be higher in inverted pavements than in conventional flexible pavements. Numerical results show that the tensile stresses in the asphalt concrete layer and in the cement-treated base, as well as the compressive stress on the subgrade, decrease as the stiffness of the unbound granular base increases.

References

Abbas, A. R., Papagiannakis, A. T., and Masad, E. A. (2004). "Linear and nonlinear viscoelastic analysis of the microstructure of asphalt concretes." *J. Mater. Civ. Eng.*, 16(2), 133–139.

Adu-Osei, A., Little, D. N., and Lytton, R. L. (2001). "Cross-anisotropic characterization of unbound granular materials." *Transportation Research Record 1757*, Transportation Research Board, Washington, DC, 82–91.

Allen, J. J., and Thompson, M. R. (1974). "Resilient response of granular materials subjected to time dependent lateral stresses." *Transportation Research Record 510*, Transportation Research Board, Washington, DC, 173–182.

Arnold, G., Dawson, A., Hughes, D., and Robinson, D. (2002). "The application of shakedown approach to granular pavement layers." *Proc., 9th Int. Conf. on Asphalt Pavements*, International Society for Asphalt Pavements, Copenhagen, Denmark.

Balbo, J. T. (1997). "High quality cement treated crushed stones for concrete pavement bases." 6th Purdue Conference on Concrete Pavement. *Proc., 6th Int. Conf. on Concrete Pavement Design and Materials for High Performance*, International Society for Concrete Pavements, Indianapolis.

Barksdale, R. D., Brown, S. F., and Chan, F. (1989). "Potential benefits of geosynthetics in flexible pavements: Supplement." National Cooperative Highway Research Program, Washington, DC.

Barksdale, R. D., and Itani, S. Y. (1989). "Influence of aggregate shape on base behavior." *Transportation Research Record 1227*, Transportation Research Board, Washington, DC, 173–182.

Brown, S. F., and Pappin, J. W. (1981). "Analysis of pavements with granular bases." *Transportation Research Record 810*, Transportation Research Board, Washington, DC, 17–23.

Brown, S. F., and Pappin, J. W. (1985). "Modeling of granular materials in pavements." *Transportation Research Record 1022*, Transportation Research Board, Washington, DC, 45–51.

Brunton, J. M., and De Almeida, J. R. (1992). "Modeling material nonlinearity in a pavement backcalculation procedure." *Transportation Research Record 1377*, Transportation Research Board, Washington, DC, 99–106.

Chen, D. H., Zaman, M., Laguros, J., and Soltani, A. (1995). "Assessment of computer programs for analysis of flexible pavement structure." *Transportation Research Record 1482*, Transportation Research Board, Washington, DC, 123–133.

Cho, Y. H., McCullough, B., and Weissmann, J. (1996). "Considerations on finite-element method application in pavement structural analysis." *Transportation Research Record 1539*, Transportation Research Board, Washington, DC, 96–101.

Dawson, A. R., Thom, N. H., and Paute, J. L. (1996). "Mechanical characteristics of unbound granular materials as a function of condition." *Proc., Flexible Pavements, Eur. Symp. Euroflex 1993*, CRC/Balkema, Rotterdam, the Netherlands.

García-Rojo, R., and Herrmann, H. J. (2005). "Shakedown of unbound granular material." *Granular Matter*, 7(2–3), 109–118.

Habiballah, T., and Chazallon, C. (2005). "An elastoplastic model based on the shakedown concept for flexible pavements unbound granular materials." *Int. J. Numer. Anal. Methods Geomech.*, 29(6), 577–596.

Hardin, B. O., and Blandford, G. E. (1989). "Elasticity of particulate materials." *J. Geotech. Eng.*, 115(6), 788–805.

Harichandran, R. S., Yeh, M. S., and Baladi, G. Y. (1990). "MICH-PAVE: A nonlinear finite element program for the analysis of flexible pavements." *Transportation Research Record 1286*, Transportation Research Board, Washington, DC, 123–131.

Hicks, R. G. (1970). "Factors influencing the resilient properties of granular materials." Ph.D. thesis, Institute of Transportation and Traffic Engineering, Univ. of California at Berkeley, Berkeley, CA.

Hicks, R. G., and Monismith, C. L. (1971). "Factors influencing the resilient response of granular materials." *Highway Res. Rec.*, 345, 15–31.

Hjelmstad, K. D., and Taciroglu, E. (2000). "Analysis and implementation of resilient modulus models for granular solids." *J. Eng. Mech.*, 126(8), 821–830.

Huurman, M. (1996). "Development of traffic induced permanent strain in concrete block pavements." *Heron*, 41(1), 29–52.

Jorenby, B. N., and Hicks, R. G. (1986). "Base course contamination limits." *Transportation Research Record 1095*, Transportation Research Board, Washington, DC, 86–101.

Kim, M. (2007). "Three-dimensional finite element analysis of flexible pavements considering nonlinear pavement foundation behavior." Ph.D. thesis, Dept. of Civil Engineering, Univ. of Illinois at Urbana-Champaign, Urbana-Champaign, IL.

Kim, M., Tutumluer, E., and Kwon, J. (2009). "Nonlinear pavement foundation modeling for three-dimensional finite-element analysis of flexible pavements." *Int. J. Geomech.*, 9(5), 195–208.

Kim, S. H., Little, D. N., and Masad, E. (2005). "Simple methods to estimate inherent and stress-induced anisotropy of aggregate base." *Transportation Research Record 1913*, Transportation Research Board, Washington, DC, 24–31.

Kim, Y. R. (2008). *Modeling of asphalt concrete.*, McGraw-Hill Professional, New York.

Kolisoja, P. (1997). "Resilient deformation characteristics of granular materials." Ph.D. thesis, Tampere Univ. of Technology, Tampere, Finland.

Kopperman, S. E., Stokoe, K. H., and Knox, D. P. (1982). "Effect of state of stress on velocity of low amplitude compression waves propagating along principal stress directions in dry sand." Univ. of Texas, Austin, TX.

Lekarp, F., Isacsson, U., and Dawson, A. (2000). "State of the art. I: Resilient response of unbound aggregates." *J. Transp. Eng.*, 126(1), 66–75.

Morgan, J. R. (1966). "The response of granular materials to repeated loading." *Proc., 3rd Conf.*, Australian Road Research Board, Sydney.

National Cooperative Highway Research Program (NCHRP). (2004). "Guide for mechanistic-empirical design of new and rehabilitated structures." *NCHRP Report 01-37A*, Transportation Research Board, Washington, DC.

Park, S. W., and Lytton, R. L. (2004). "Effect of stress-dependent modulus and Poisson's ratio on structural responses in thin asphalt pavements." *J. Transp. Eng.*, 130(3), 387–394.

Pennington, D. S., Nash, D. F. T., and Lings, M. L. (1997). "Anisotropy of G_0 shear stiffness in gault clay." *Geotechnique*, 47(3), 391–398.

Raad, L., and Figueroa, J. L. (1980). "Load response of transportation support systems." *Transp. Eng. J.*, 106(1), 111–128.

Rada, G., and Witczak, M. W. (1981). "Comprehensive evaluation of laboratory resilient moduli results for granular material." *Transportation Research Record 810*, Transportation Research Board, Washington, DC, 23–33.

Richardson, D. N., and Lusher, S. M. (2008). *Determination of creep compliance and tensile strength of hot mix asphalt for wearing courses in Missouri*, *Final Rep. RI05-052*, Missouri Dept. of Transportation, Jefferson City, MO.

Robinson, R. G. (1974). "Measurement of the elastic properties of granular materials using a resonance method." *Supplementary Report No. 111UC*, Transport and Road Research Laboratory, Berkshire, England.

Santamarina, J. C., and Fratta, D. (2005). *Discrete signals and inverse problems: An introduction for engineers and scientists*, Wiley, Chichester, UK.

Santamarina, J. C., Klein, K. A., and Fam, M. A. (2001). *Soils and waves*, Wiley, New York.

Shifley, L. H., and Monismith, C. L. (1968). "Test road to determine the influence of subgrade characteristics on the transient deflections of asphalt concrete pavements." Materials and Research Dept. Division of Highways State of California, Berkeley, CA.

Smith, W. S., and Nair, K. (1973). "Development of procedures for characterization of untreated granular base coarse and asphalt-treated base course materials." Federal Highway Administration, Washington, DC.

Sukumaran, B., Chamala, N., Willis, M., Davis, J., Jurewicz, S., and Kyatham, V. (2004). "Three dimensional finite element modeling of flexible pavements." *Proc., Worldwide Airport Technology Transfer Conf.*, Federal Aviation Administration, Washington, DC.

Tao, M., Mohammad, L. N., Nazzal, M. D., Zhang, Z., and Wu, Z. (2010). "Application of shakedown theory in characterizing traditional and recycled pavement base materials." *J. Transp. Eng.*, 136(3), 214–222.

Theyse, H., De Beer, M., and Rust, F. (1996). "Overview of South African mechanistic pavement design method." *Transportation Research*

Record 1539, Transportation Research Board, Washington, DC, 6–17.

Thom, N. H., and Brown, S. F. (1988). "The effect of grading and density on the mechanical properties of a crushed dolomitic limestone." *Proc., 14th Conf.*, Australian Road Research Board, Sydney.

Trollope, E. H., Lee, I. K., and Morris, J. (1962). "Stresses and deformation in two-layer pavement structures under slow repeated loading." *Proc., 1st Conf.*, Australian Road Research Board, Sydney.

Tutumluer, E. (1995). "Predicting behavior of flexible pavements with granular bases." Ph.D. thesis, School of Civil and Environmental Engineering, Georgia Institute of Technology. Atlanta, GA.

Tutumluer, E., and Barksdale, R. D. (1995). "Inverted flexible pavement response and performance." *Transportation Research Record 1482*, Transportation Research Board, Washington, DC, 102–110.

Underwood, S., Heidari, A., Guddati, M., and Kim, Y. (2005). "Experimental investigation of anisotropy in asphalt concrete." *Transportation Research Record 1929*, Transportation Research Board, Washington, DC, 238–247.

Uzan, J. (2005). "Viscoelastic-viscoplastic model with damage for asphalt concrete." *J. Mater. Civ. Eng.*, 17(5), 528–534.

Van Niekerk, A. A., Molenaar, A. A. A., and Houben, L. J. M. (2002). "Effect of material quality and compaction on the mechanical behaviour of base course materials and pavement performance." *Proc., 6th Int. Conf. on Bearing Capacity of Roads, Railways and Airfields*, Taylor & Francis, Lisbon, Portugal.

Werkmeister, S., Dawson, A. R., and Wellner, F. (2004). "Pavement design model for unbound granular materials." *J. Transp. Eng.*, 130(5), 665–674.

J. Transp. Eng. 2012.138:1507-1519.